HEALTH AND MEDICINE

Interaction network of extracellular vesicles building universal analysis via eye tears: iNEBULA

Liang Hu[1,2]†, Xiaoling Liu[1,2]†, Qiaolan Zheng[2], Wuhe Chen[2], Hao Xu[1,2], Hengrui Li[1,2], Jiaxin Luo[1,2], Rui Yang[1,2], Xulong Mao[3], Siyao Wang[1,2], Tucan Chen[1,2], Luke P. Lee[4,5,6,7]*, Fei Liu[1,2]*

Discovering the secrets of diseases from tear extracellular vesicles (EVs) is well-recognized and appreciated. However, a precise understanding of the interaction network between EV populations and their biogenesis from our body requires more in-depth and systematic analysis. Here, we report the biological profiles of different-size tear EV subsets from healthy individuals and the origins of EV proteins. We have identified about 1800 proteins and revealed the preferential differences in the biogenesis among distinct subsets. We observe that eye-related proteins that maintain retinal homeostasis and regulate inflammation are preferentially enriched in medium-size EVs (100 to 200 nm) fractions. Using universal analysis in combination with the Human Protein Atlas consensus dataset, we found the genesis of tear EV proteins with 37 tissues and 79 cell types. The proteins related to retinal neuronal cells, glial cells, and blood and immune cells are selectively enriched among EV subsets. Our studies in heterogeneous tear EVs provide building blocks for future transformative precision molecular diagnostics and therapeutics.

INTRODUCTION

Extracellular vesicles (EVs) can be shed from almost all tissues and cells to shuttle intercellular signals and effector molecules via circulating body fluids, making them essential sources in medical diagnostics and therapeutics. Now, EVs are predominantly classified as exosomes (30 to 150 nm) originating from the endosome, microvesicles (150 to 1000 nm) budding from the plasma membrane, and apoptotic bodies (200 to 5000 nm) released during apoptosis (1, 2). Despite the homogeneous lipid bilayers of EV subsets, cargos including proteins, RNAs, and metabolites are selectively packaged into EV subpopulations, playing distinct roles in intercellular communication (2). Thus, understanding the heterogeneous nature of EV compositions and biofunctions is critical for their development as clinical biomarkers and therapeutic carriers. To date, increasing efforts have been made to deconstruct the EV subsets that are found principally in cell culture medium (3), plasma (4), and urine (5). With these biofluid sources, the distinct molecular profiles, biological and biophysical properties, and organ biodistribution patterns of EV subpopulations have been demonstrated by analyzing their secretome landscapes.

By detecting and transforming views via neuronal signals to the brain's visual centers, our ocular system allows us to see and activate the inner emotional response (6). Human tears, serving as a liquid barrier for maintaining and protecting ocular health, have been considered EV sources for liquid biopsy resembling blood (7). Notably, the value of tear analysis can be extended beyond the ocular system. It is because tears are secreted by the lacrimal glands, which contain enriched biological molecules filtrated from the circulating blood system. Therefore, tears carry rich bioinformation from other seemingly unrelated body organs (8). Studies using bulk tear EV have shown this value by estimating their capabilities in discerning the pathological changes of the ocular system [e.g., dry eye (9) and glaucoma (10)] and non-ocular tissues [e.g., breast cancer (11), prostate cancer (12), and multiple sclerosis (13)]. Nevertheless, although most, if not all, of the protein components in tear EVs have been described, the information regarding subset distribution patterns still needs to be determined, especially because the interaction network between tear EV subgroups and human tissues still needs to be seen. To share insights into the biological connections of tear EV subsets and the origins of EV proteins in the visual system (Fig. 1A), in this study, we report a resource depicting the Interaction Network of Extracellular Vesicles Building Universal Analysis via Eye Tears (iNEBULA).

RESULTS

### Synchronized preparation of different-size EV subsets

We first prepared tear EV populations with distinct size ranges via our recently established tool (14, 15). We highlighted the diversity of tear EVs with wide size distribution and multimodal peak profile (fig. S1A), and have observed comparable quantitative results of particles among healthy individuals (fig. S1, B and C). We then separated the different-size EV subpopulations that were defined as small EVs (sEVs; 20 to 100 nm), medium EVs (mEVs; 100 to 200 nm), and large EVs (lEVs; 200 to 450 nm) fractions. Evident size clustering and peak shifting could be depicted among the distinct EV subgroups (mode size of 101, 141, and 204 nm for sEV, mEV, and lEV fractions, respectively) (fig. S2A). At the same time, the particle and protein levels showed little difference (fig. S2, B, and C). We also used transmission electron microscopy (TEM)

[1]National Engineering Research Center of Ophthalmology and Optometry, Eye Hospital, Wenzhou Medical University, Wenzhou 325027, China. [2]National Clinical Research Center for Ocular Diseases, Eye Hospital, Wenzhou Medical University, Wenzhou 325027, China. [3]The First Affiliated Hospital of Wenzhou Medical University, Wenzhou 325000, China. [4]Renal Division and Division of Engineering in Medicine, Department of Medicine, Brigham and Women's Hospital, Harvard Medical School, Boston, MA 02115, USA. [5]Department of Bioengineering, University of California at Berkeley, Berkeley, CA 94720, USA. [6]Department of Electrical Engineering and Computer Science, University of California at Berkeley, Berkeley, CA 94720, USA. [7]Institute of Quantum Biophysics, Department of Biophysics, Sungkyunkwan University, Suwon, Gyeonggi-do 16419, Korea.
†These authors contributed equally to this work.
*Corresponding author. Email: lplee@bwh.harvard.edu (L. P. L.); feiliu@wmu.edu.cn (F. L.)
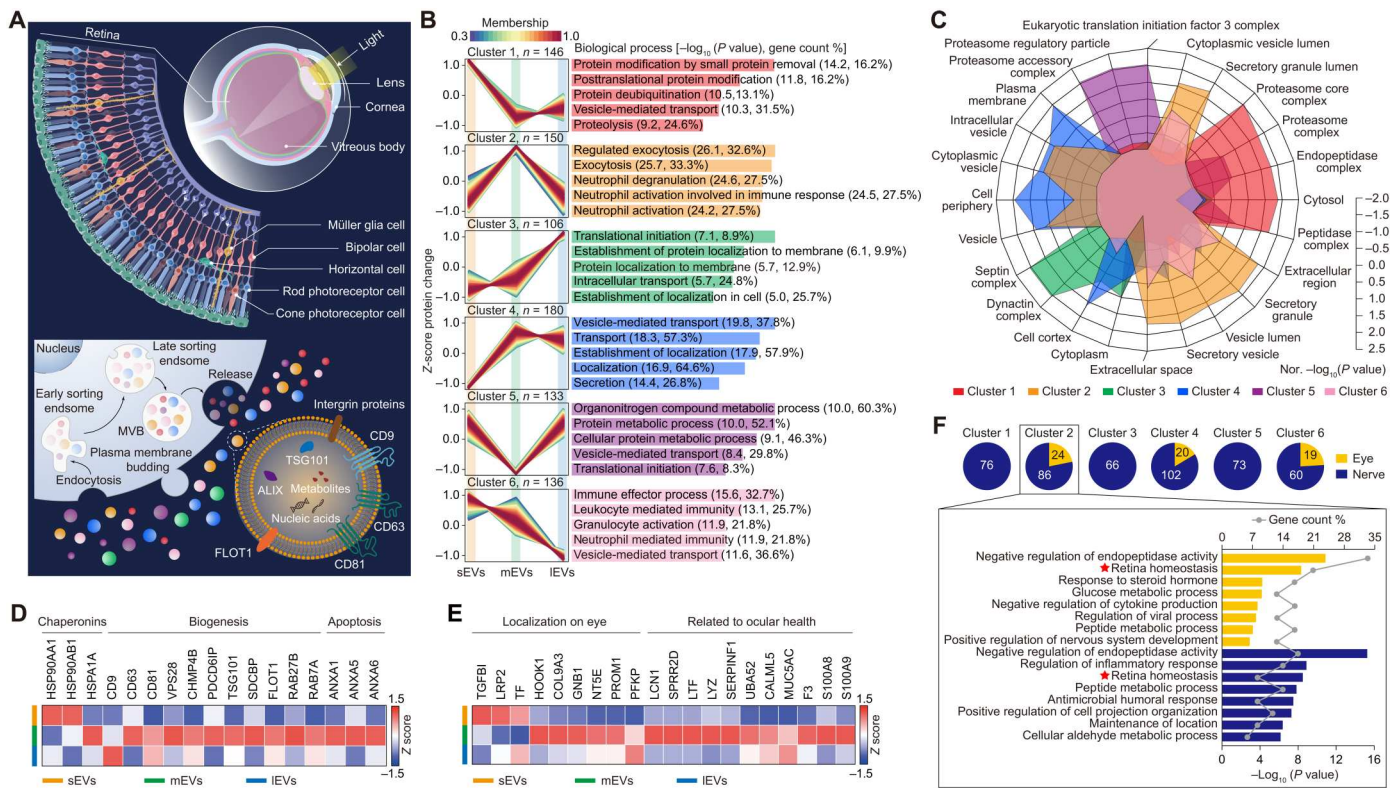
Fig. 1. The composition and biofunction profiles of tear EV subsets. (**A**) Schematic illustration of tear-derived EVs in the visual system. Exosomes originate from the endosomal pathway and are released after the fusion of multivesicular bodies (MVBs) with the plasma membrane. Microvesicles are released through plasma membrane budding. (**B**) Cluster patterns (left) and top 5 biological processes (right) of cluster proteins. The proteins with relatively higher abundance in the sEVs (20 to 100 nm) were included in clusters 1, 5, and 6, while clusters 2, 4, and 6 for mEVs (100 to 200 nm) and clusters 3, 4, and 5 for lEVs (200 to 450 nm). (**C**) Radar graph of the top 5 cellular components in the six clusters of the three EV subsets. The Z-score assessment was used for normalization (Nor.). (**D**) Heatmap of the relative abundance of identified EV proteins among subgroups. The scale indicates Z-score–transformed intensity. (**E**) Heatmap of the relative abundance of the visual system–related proteins in tear EV subsets. (**F**) Top 8 biological functions of the visual system–related proteins from cluster 2. VPS28, vacuolar protein sorting–associated protein 28 homolog; CHMP4B, charged multivesicular body protein 4b; PDCD6IP, programmed cell death 6 interacting protein; TSG101, tumor susceptibility gene 101 protein; SDCBP, syndecan binding protein; FLOT1, flotillin-1; RAB27B, Ras-related protein Rab-27B; RAB7A, Ras-related protein Rab-7a; ANXA1/A5/A6, annexin A1/A5/A6; TGFBI, transforming growth factor-beta- induced protein ig-h3; LRP2, low-density lipoprotein receptor(LDL)–related protein 2; TF, transferrin; HOOK, protein Hook homolog 1; COL9A3, collagen alpha-3(IX) chain; GNB1, guanine nucleotide-binding protein G(I)/G(S)/G(T) subunit beta-1; NT5E, 5'-nucleotidase; PROM1, prominin-1; PFKP, ATP-dependent 6-phosphofructokinase, platelet type; LCN1, lipocalin-1; SPRR2D, small proline-rich protein 2D; LTF, lactotransferrin; LYZ, lysozyme C; SERPINF1, serpin family F member 1; UBA52, ubiquitin-60S ribosomal protein L40; CALML5, calmodulin-like protein 5; MUC5AC, mucin-5AC.

imaging to compare their size and morphology. Although the size overlaps between each EV subgroup to some extent (fig. S2A), TEM images evidenced a bona fide property of distinct EV particle size ranges (fig. S2D). Besides, we found that the medium-size fractions were rich in cup-shaped vesicles of morphology consistent with exosomal properties. We lastly evaluated the exosome-specific proteins in EV subsets by Western blot (WB) because nanoscale exosomes are a vital component of EVs. Most groups could be detected with classical exosomal markers without obvious albumin contamination (fig. S3).

## Mapping the biofunctions and origins of tear EV subsets within the ocular system

We first investigated the coexpression clusters and biological processes involved in the differentially expressed proteins among sEVs, mEVs, and lEVs. With a comprehensive proteomic analysis of EV subsets from the tear pool of 38 healthy human subjects, we identified 1815, 1829, and 1892 proteins from sEV, mEV, and

lEV fractions, respectively, in which 1470 proteins were quantifiable (fig. S4). We found six distributional trajectories of coexpressed proteins (Fig. 1B and table S2), demonstrating subset-specific clusters with high- or low-abundance proteins. Expectedly, we found an enrichment of proteins related to vesicle-mediated transport in all three EV subgroups (table S3). The proteins participating in the protein modification and biological metabolism processes, such as small protein removal and organonitrogen compound metabolic process, were relatively highly abundant in the sEVs (corresponding to clusters 1, 5, and 6). Proteins associated with immune response and immunoregulation functions were preferentially enriched in the mEVs (clusters 2, 4, and 6), while more plasma membrane assembly- and translation initiation-associated proteins were packaged in lEVs (clusters 3, 4, and 5). The above results suggested that transportation of the intracellular proteins via EV subsets contributes to various biofunctions.

We then compared the cellular components to understand the differently sized EVs biogenesis and cargo sorting. Specifically,

extracellular-related proteins were mainly loaded by mEVs, while proteasome- and cytoplasm-associated components were substantially more enriched in sEVs and lEVs clusters (Fig. 1C, fig. S5, and table S4). Previous studies (16–18) have demonstrated that exosomal protein sorting and loading occur at the endosomal system,

relying on the tetraspanin CD63, syndecan binding protein (SDCBP; synonyms: Syntenin-1), and flotillin-1 (FLOT1) , as well as components of the endosomal sorting complex required for transport (ESCRT) complex, such as tumor susceptibility gene 101 protein (TSG101), programmed cell death 6 interacting
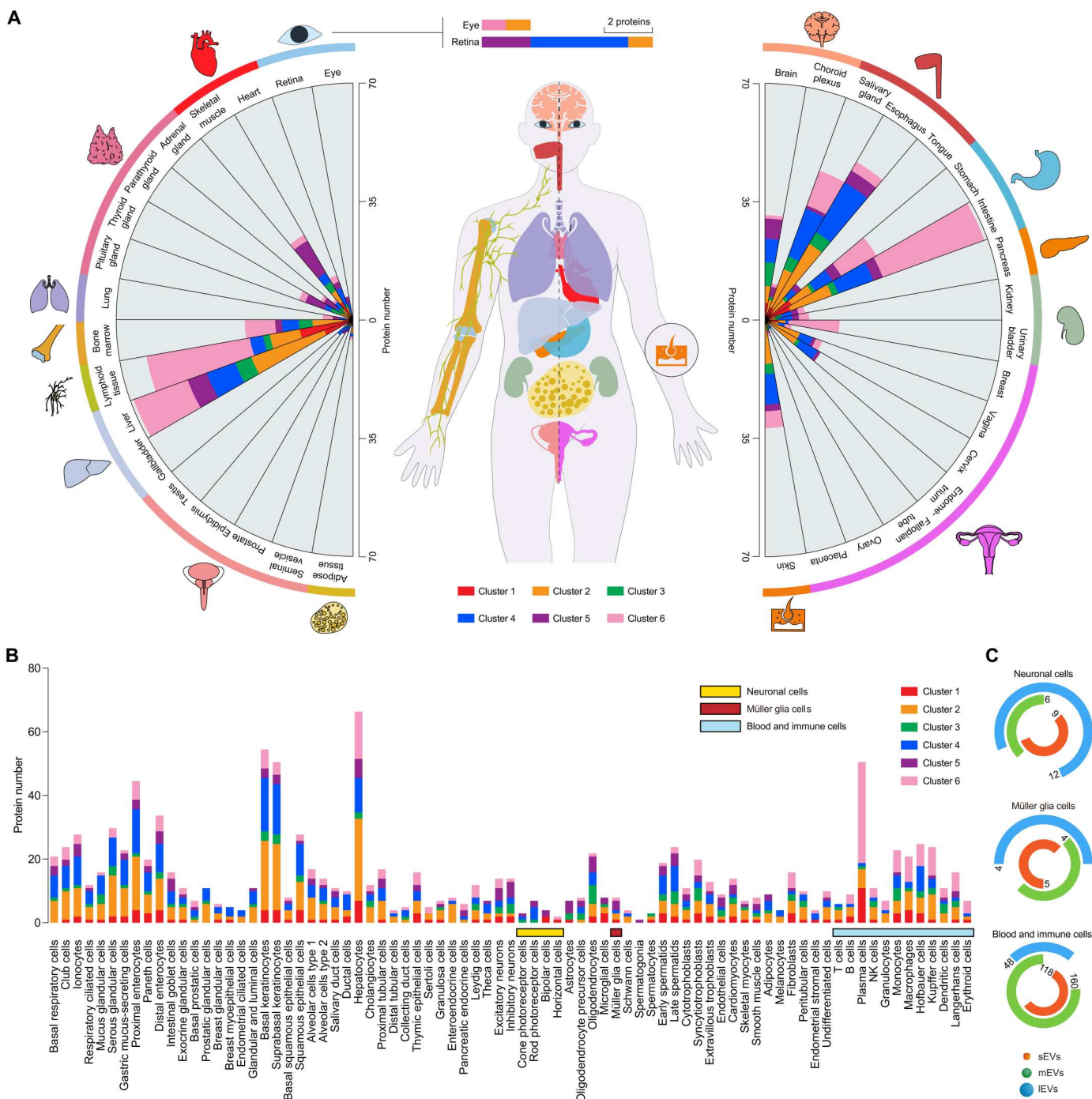
Fig. 2. Tissue and cell type origin of the tear EV proteins. (**A**) Detection of tissue-specific proteins among clusters of differentially abundant proteins. (**B**) Detection of cell type–specific proteins in clusters of tear EVs. (**C**) Distributions of the proteins among the different EV subsets, focusing on those specific to eye-related neuronal cells, müller glial cells, and blood and immune cells. The intersection of the quantifiable proteins in tear EVs with tissue- and cell type–specific proteins (or genes) from the Human Protein Atlas (HPA) dataset. The particular tissue/cell type–enhanced, group-enriched, and tissue/cell type–enriched proteins in the HPA dataset are defined as tissue- or cell type–specific proteins. NK, natural killer.

protein (PDCD6IP, synonyms: Alix), and charged multivesicular body protein 4b (CHMP4B). We observed higher enrichment of these proteins within mEVs (Fig. 1D), suggesting that an endosomal pathway might be required for cargo selection for this subset of EVs. Meanwhile, the abundance of the annexin A1/A5/A6 (ANXA1/A5/A6) proteins, related to apoptotic processes (*19–21*), was higher in the mEVs and lEVs. In contrast, chaperonins, such as heat shock proteins, were more enriched in sEVs and mEVs. These results were suggestive of fundamental differences in the biogenesis among tear EVs subsets; however, the role of a specific protein as regulating factor for subset-specific cargo sorting remains further investigated.

Enriching tissue-derived EVs is encouraged, as it can provide the possibility of direct monitoring the tissue abnormality without collecting the tissue (*22*). Because the lacrimal glands are anatomically adjacent to the visual system (including the eye, optic nerve, and visual cortex), we first investigated the proteins originating from the visual system that the three EV subsets may selectively carry. We found the elevated abundance of some proteins in mEVs, including potential markers for the diagnosis of ocular disease [e.g., lactotransferrin (LTF), lipocalin-1 (LCN1), lysozyme C (LYZ), calmodulin-like protein 5 (MUC5AC), and small proline-rich protein 2D (SPRR2D)] (*23–25*), as well as components responsible for protein modification [ubiquitin-60*S* ribosomal protein L40 (UBA52)] (*26*), coagulation [tissue factor (F3)] (*27*), neuroprotection [serpin family F member 1 (SERPINF1)] (*28*), and inflammatory responses (S100A8 and S100A9) (*29*) (Fig. 1E). Subsequent examination of the tissue locations using the STRING database demonstrated eye-related annotations mainly in the clusters of mEV-enriched proteins (Fig. 1F and table S5). Among the proteins associated with the eye and nerve, only cluster 2 components (proteins most enriched in mEVs) were found to have roles in retinal homeostasis (Fig. 1F and tables S6 and S7), revealing the importance of characterizing this EV subset for ophthalmic research. As tear EV markers and cargos with eye origins showed an mEV synchronous pattern, we thus speculated that the preferential packaging of ocular proteins is probably dependent on the multivesicular endosome biogenesis pathway.

To globally understand the interaction networks of tear EVs with the human body, we then analyze the tissue and cell contributions of these secretory proteins by using the Human Protein Atlas [HPA; based on immunohistochemistry or single-cell RNA sequencing (RNA-seq) analysis] consensus dataset (*30–32*). Regarding the overall assessment, we first analyzed the quantifiable proteins carried by tear EVs and found that they were annotated to 37 tissues and 79 cell types (fig. S6). We further investigated the tissue origins of differentially expressed proteins among EV subpopulations. In addition to the lacrimal gland–specific proteins in Fig. 1E (e.g., LTF, LCN1, and LYZ) (*33*), 2 and 7 proteins that were respectively identified as eye- and retina-specific proteins in the HPA dataset (recognized by immunohistochemistry or RNA-seq in the cornea, vitreous body, and retina) were found differential expressions among tear EV subsets (Fig. 2A). These ocular system–specific proteins were more enriched in mEVs and lEVs than in sEVs. We lastly used the HPA single-cell RNA profiles based on tissue-specific data to explore the distribution of EV proteins relating to the circulating plasma cells, immune cells, and retina neuronal cells. We found that lEVs contain relatively more proteins originating from eye-specific neuronal cells including cone

photoreceptor cells, rod photoreceptor cells, bipolar cells, and horizontal cells, while müller glia cell proteins showed little differences among all EV subsets (Fig. 2, B and C). In addition, proteins relevant to blood and immune cells were sorted more into sEVs and mEVs (Fig. 2C), suggesting a closer connection of smaller-size EVs with the circulation system.

Distinct fingerprint profiles of tear EV fractions
Last, we used matrix-assisted laser desorption/ionization–time-of-flight mass spectrometry (MALDI-TOF MS) fingerprints for discriminating the tear-derived EV subfractions for validation. The fingerprints of the EV subsets were compared based on the relative intensities of peaks that originated mainly from proteins with a mass range of 2000 to 20,000 mass/charge ratios (m/z) (fig. S7A). The averaged fingerprints from the individual trials revealed distinct profiles across the three subsets (fig. S7B). Protein abundance showed a higher correlation between sEVs and mEVs (fig. S7C). The principal components analysis (PCA) scores further suggested the distinct protein compositions of the EV subpopulations (fig. S7D). A series of differentiating peaks from the three subsets were found (table S8), and two strong specific peaks with repeatable signals were further selected at *m/z* of 7719 and 14,654, which can be served as potential markers for subset classification (fig. S7E). In addition, these two peaks were observed relatively higher abundance in the mEV subpopulation (fig. S7F). Following conjoint analysis of the proteomics data, proteins matching the molecular mass (SPRR2D of 7.9 kDa and UBA52 of 14.7 kDa) were extrapolated to be potentially consistent with the observed pattern in MALDI fingerprints (fig. S7, G and H), that is, showing the highest relative intensities in the mEV pool.

DISCUSSION
Despite mounting methodologies for deconstructing EV subpopulations from various biological fluids, more is needed regarding the heterogeneity of EVs in human tears. In this work, we successfully separated the tear EV subsets with different sizes and contents, owing to the favorable performance of the established isolation tool in manipulating the small volume tear sample and separating different-size particles. The measurements in the physical parameters of the nanoparticles indicated that the particles in the small-size group were more homogeneous than those in the larger fractions. In addition, the broadening and positive offset of the particle size distribution were observed in the nanoparticle tracking analysis (NTA) results compared with those of TEM, probably due to vesicle aggregation, signal enhancement induced by microsampling, and the detection limit of NTA. WB analysis demonstrated that tetraspanin markers (CD63 and CD9) and exosomal component mac-2 binding protein (Mac-2BP) showed a preferential expression in those fractions with smaller sizes, although they could be consistently detected in all subsets. Alix, an ESCRT-associated protein (*34*), was not detected in large particles. Heat shock protein HSP90, a presumed exomere (*35*) (depicted as membrane-free nanoparticles) marker, was readily detectable in small and medium rather than large fractions.

Our differential proteomic analysis further revealed that the mEV subpopulation contained more proteins associated with exosomal biogenesis than the other two productions. High enrichment of proteins for plasma membrane localization and cytoplasm

composition was present in lEVs, extrapolating a possible subcellular origin of these particles through plasma membrane budding. A unique protein distribution was also revealed in mEVs, in which the histologic origins and biological functions of the proteins exhibited a close correlation with visual sense and ocular health. Tissue factor that was well-demonstrated abundance in tear EVs (36) and lysosome-associated membrane glycoprotein 2 (LAMP2) that plays essential roles in retinal pigment epithelium biology (37) were further noted to be preferentially enriched within mEVs (table S1). The recent study also suggested an ESCRT-independent manner using LAMP2A (isoform A of LAMP2) to regulate the protein loading into the exosomes (38). In addition, we found that the proteins related to the immune organs (lymphoid tissue and bone marrow), as well as the immune cell (e.g., T cells, B cells, natural killer cells, granulocytes, monocytes, macrophages, and dendritic cells), showed higher intensities in smaller size EVs, particularly mEVs (Fig. 2, A and B), further suggesting the potential roles of medium-size EVs in participating in immunomodulation in the visual system. Noticeably, the consensus has yet to emerge on specific markers of EV subsets [the Minimal Information for Studies of Extracellular Vesicles 2018 (1)]. Nevertheless, our observations provide useful evidences for deconstructing the heterogeneous protein compositions and functional preferences among different-size EV subpopulations in human tears.

The fingerprints of the intact EV particles were also generated by MALDI-TOF MS. Both MS peaks and the PCA scores based on these peaks suggested the feasibility of our established tools for separating tear EV subpopulations with distinct protein compositions. Because proteins of 2000 to 20,000 m/z are easier to ionize (39, 40), the EV components within this mass range were mainly detected. Among these peaks, we found two differential MALDI peaks (7719 and 14,654 m/z) with the most abundant signals in the subgroup of 100 to 200 nm, which showed a similar expression pattern with liquid chromatography with tandem MS (LC-MS/MS) results of SPRR2D and UBA52. This finding also revealed the potential role of the medium-size tear EVs as the biomarker resources for ocular disorders, which has been supported by previous reports demonstrating the accumulation of SPRR2 in the conjunctival epithelium of the dry eye (24) and the role of the ubiquitin-proteasome system in the clearance of pathogenic proteins of neurodegeneration (26).

In conclusion, we have developed an iNEBULA that can provide evidence of the heterogeneous protein compositions and functions of different-size EV subpopulations in human tears. We have systematically identified that visual system–related proteins are preferentially loaded into mEVs and play crucial roles in maintaining retinal homeostasis and regulating inflammation. Unraveling the protein components and functional outcomes and better understanding the heterogeneity among tear-derived EV subsets with large-scale clinical cohorts is encouraged in the future, promoting tear-based diagnostics and therapeutics.

MATERIALS AND METHODS
Collection of tear fluid samples
Tear samples were obtained from healthy donors (aged 18 to 42 years) following the protocols approved by the Research Ethics Committee at the Eye Hospital of Wenzhou Medical University (2020-203-k-185-01). Informed consent was obtained from all human subjects. The tear fluid was collected by placing the Schirmer test strips (Jingming, China) in the lower lid for 5 to 10 min at room temperature (RT), and the imbibed strips from both two eyes were subsequently transferred to 2 ml of 10 mM phosphate-buffered saline (PBS; Thermo Fisher Scientific). The eluted tear fluid was centrifuged at 300g for 10 min and at 2000g for 10 min to remove cells and debris. Unless otherwise indicated, a tear sample from the individual was collected six times and pooled as the final suspension.

Isolation of tear EV subpopulations
After a 0.45-μm prefiltration step, tear suspension was isolated based on the EXODUS method (15) under an alternative vacuum actuation with the experimental condition of −20 kPa and 10-s conversion time. Following isolation, each subfraction was further eluted twice with PBS via EXODUS. Last, the reserved three fractions were recovered in 200 μl of PBS and stored at −80°C for subsequent analysis.

Nanoparticle tracking analysis
Size distribution and concentration of the tear EV subtypes were measured using a NanoSight NS300 (Malvern) equipped with a 488 nm laser. Before NTA detection, the samples were diluted in PBS. Each sample was analyzed by recording 30-s videos in three replicates with optimal set parameters (the detection threshold of 15). For consistency, all NTA measurements were performed with a syringe pump (the speed used was 30 μl/min).

Transmission electron microscopy
TEM imaging was conducted to observe the morphology of the tear EV subtypes. Specifically, a 40 μl of sample solution with an equal volume of 4% paraformaldehyde was spotted on a piece of parafilm, followed by its absorption with the formvar/carbon copper grids for 30 min. Following PBS washing, the sample on the grid was fixed with 1% glutaraldehyde for 5 min, negatively stained with 2% uranyl acetate for 30 s, and left to air dry. Imaging was lastly performed with a transmission electron microscope at 200 kV (Talos F200S, Thermo Fisher Scientific).

Protein immunoblotting
WB detection was performed using samples with an equal protein mass (3 μg; measured by Qubit Protein Assay Kits), which were loaded onto a 4 to 20% precast polyacrylamide slab mini-gel for electrophoresis, and subsequently transferred onto a polyvinylidene fluoride membrane by Trans-Blot Turbo Transfer System (Bio-Rad). The membranes were blocked with 5% nonfat dry milk in PBS containing 0.1% Tween 20 at RT for 1 hour, followed by primary antibody incubation overnight at 4°C. After PBS washing, the membranes were immersed in horseradish peroxidase (HRP)–conjugated anti-mouse immunoglobulin G (IgG) (7076, Cell Signaling Technology) or HRP-conjugated anti-rabbit IgG (7074, Cell Signaling Technology) at RT for 60 min. The images were performed using enhanced chemiluminescence for immunodetection (Peiqing Science & Technology). All the primary antibodies were diluted to 1:1000, whereas the secondary antibodies were diluted to 1:3000. The primary antibodies used for WB included the following: anti-Alix (sc-53540, Santa Cruz Biotechnology), anti–Mac-2BP (sc-374541, Santa Cruz Biotechnology), anti-HSP90 (sc-69703, Santa Cruz Biotechnology), anti-CD63

(ab134045, Abcam), anti-CD9 (sc-13118, Santa Cruz Biotechnology), and anti-albumin (ab151742, Abcam).

LC-MS/MS and proteomic analysis

The EV subpopulations (size range of 20 to 100, 100 to 200, and 200 to 450 nm) from the pooled tear sample were isolated via EXODUS, and an equal amount of each sample (30 μg of proteins based on bicinchoninic acid quantification; Beyotime Biotechnology) was subjected to label-free LC-MS/MS analysis. The complete list of the identified proteins is provided in table S1.

For sample preparation, lysis buffer containing 1% protease inhibitor (Merck Millipore) and 8 M urea (Sigma-Aldrich) was added to the EV sample, followed by ultrasonic lysis. The protein solution was reduced with 5 mM dithiothreitol (Sigma-Aldrich) at 56°C for 30 min and alkylated with 11 mM iodoacetamide (Sigma-Aldrich) in the dark at RT for 15 min. Following dilution of the lysate with tetraethylammonium bromide (Sigma-Aldrich) to reduce the urea concentration below 2 M, trypsin (Promega) was added at a ratio of 1:50 (w:w) for digestion at 37°C overnight. A second treatment with trypsin (mass ratio of 1:100) was performed for the subsequent 4-hour incubation.

For LC-MS/MS, the peptides were analyzed on an OrbitrapExploris 480 mass spectrometer (Thermo Fisher Scientific) equipped with an Easy nLC-1200 (Thermo Fisher Scientific). The mobile phase solvents included buffer A (0.1% formic acid and 2% acetonitrile; Fluka and Thermo Fisher Scientific) and buffer B (0.1% formic acid and 90% acetonitrile). The elution was achieved with a gradient buffer B (0 to 68 min, 6 to 23% B; 68 to 82 min, 23 to 32% B; 82 to 86 min, 32 to 80% B; and 86 to 90 min, 80% B) under a flow rate of 500 nl/min. The mass spectrum parameters were set as follows: ion source voltage of 2.3 kV; compensating voltage of −45 and −65 V; scanning range of primary MS and scanning resolution of 400 to 1500 m/z and 60,000, respectively; the scanning range of the secondary MS and the scanning resolution were as follows: ≥110 m/z and 15,000; TurboTMT was set at off mode. A data-dependent scan mode was used for information collection. The top 25 most abundant ions were selected for fragmentation using a 27% normalized collision energy and automatic gain control (target of 5×10^4 with a maximum injection time of auto). Dynamic exclusion was set to 20 s. Secondary MS data were retrieved by Proteome Discoverer software (v2.4.1.15, Thermo Fisher Scientific) against the *Homo sapiens* SwissProt database. The search criteria were used as follows: Peptide and fragment ion tolerances were set to 10 parts per million and 0.02 Da, respectively; minimum peptide length was set at 6; trypsin was specified as a cleavage enzyme allowing up to two missing cleavages; a static modification of carbamidomethyl on Cys and dynamic changes of oxidation (Met), acetyl (N terminus), Met-loss, Met-loss + acetyl, and deamidation (Asn and Gln) were allowed. Filtration was used with a 1% false discovery rate for peptide spectrum matches and protein quantification (requiring at least two specific peptides) to improve the data quality.

For clustering and annotation analysis, Mfuzz with fuzzy c-means algorithm (41) was used for the group identification of the quantifiable proteins (SD > 0.5), and the *H. sapiens* SwissProt database was used for Gene Ontology analysis. The tissue and cell-type origins of the proteins from distinct clusters were retrieved from the STRING database (v11.5; https://cn.string-db.org) and the HPA database (v22.0; www.proteinatlas.org). At the same time, the biological process annotations of the visual and nerve system–related proteins were obtained using the Metascape database (v3.5; https://metascape.org).

MALDI-TOF MS fingerprints

The presence of acetonitrile in the matrix aids in disorganizing the protection of the lipid bilayer. Therefore, instead of the protein extracts following lysis and labeling, EV entities could be detected directly via MALDI-TOF MS within several minutes (39). After treating EV-matrix "co-crystals" with pulsed laser irradiation and ionization in MALDI, the components were detected with ion packets according to their m/z ratios in a TOF mass analyzer. Analyte/matrix co-crystals were prepared for MALDI-TOF MS characterization: The α-Cyano-4-hydroxycinnamic acid was dissolved in TA50 (acetonitrile/water/trifluoroacetic acid with a volume percentage of 50/49.9/0.1%), which was used as the matrix. One microliter of a sample containing EV entities (more than 2×10^{10} particles/ml) was mixed with an equal matrix volume. The mixture was spotted on a MALDI target plate (Ground Steel, Bruker) and dried quickly in a vacuum before analysis. Subsequently, the target plate was loaded into a MALDI-TOF mass spectrometer (Bruker) for measurement under the linear and positive ion mode.

The mass spectrum data were analyzed using a standardized system (ClinProTools software, version 3.0) to obtain peak statistics, including relative peak intensity, average spectra calculation, and classification. To test the similarity between each two mass spectra, the similarity score was calculated by the cosine correlation method (42, 43).

Statistical analysis

Statistical comparisons were performed using a one-way analysis of variance (ANOVA) followed by Tukey's post hoc test. The data are presented as means ± SEM or means ± SD using GraphPad Prism (GraphPad Software; v8.0.1). Characteristic MALDI peaks were sorted through statistical tests of ANOVA, the Wilcoxon/Kruskal-Wallis test, and the Anderson-Darling test. A P value < 0.05 was considered to indicate a statistically significant difference.

Supplementary Materials

This PDF file includes:
Figs. S1 to S7
Legends for tables S1 to S8

Other Supplementary Material for this manuscript includes the following:
Table S1 to S8

View/request a protocol for this paper from *Bio-protocol*.

REFERENCES AND NOTES

1. C. Théry, K. W. Witwer, E. Aikawa, M. J. Alcaraz, J. D. Anderson, R. Andriantsitohaina, A. Antoniou, T. Arab, F. Archer, G. K. Atkin-Smith, D. C. Ayre, J.-M. Bach, D. Bachurski, H. Baharvand, L. Balaj, S. Baldacchino, N. N. Bauer, A. A. Baxter, M. Bebawy, C. Beckham, A. B. Zavec, A. Benmoussa, A. C. Berardi, P. Bergese, E. Bielska, C. Blenkiron, S. Bobis-Wozowicz, E. Boilard, W. Boireau, A. Bongiovanni, F. E. Borràs, S. Bosch, C. M. Boulanger, X. Breakefield, A. M. Breglio, M. Á. Brennan, D. R. Brigstock, A. Brisson, M. L. D. Broekman, J. F. Bromberg, P. Bryl-Górecka, S. Buch, A. H. Buck, D. Burger, S. Busatto, D. Buschmann, B. Bussolati, E. I. Buzás, J. B. Byrd, G. Camussi, D. R. F. Carter, S. Caruso, L. W. Chamley, Y.-

T. Chang, C. Chen, S. Chen, L. Cheng, A. R. Chin, A. Clayton, S. P. Clerici, A. Cocks, E. Cocucci, R. J. Coffey, A. Cordeiro-da-Silva, Y. Couch, F. A. W. Coumans, B. Coyle, R. Crescitelli, M. F. Criado, C. D'Souza-Schorey, S. Das, A. D. Chaudhuri, P. de Candia, E. F. De Santana, O. De Wever, H. A. del Portillo, T. Demaret, S. Deville, A. Devitt, B. Dhondt, D. Di Vizio, L. C. Dieterich, V. Dolo, A. P. D. Rubio, M. Dominici, M. R. Dourado, T. A. P. Driedonks, F. V. Duarte, H. M. Duncan, R. M. Eichenberger, S. Ekström, S. El Andaloussi, C. Elie-Caille, U. Erdbrügger, J. M. Falcón-Pérez, F. Fatima, J. E. Fish, M. Flores-Bellver, A. Försönits, A. Frelet-Barrand, F. Fricke, G. Fuhrmann, S. Gabrielsson, A. Gámez-Valero, C. Gardiner, K. Gärtner, R. Gaudin, Y. S. Gho, B. Giebel, C. Gilbert, M. Gimona, I. Giusti, D. C. I. Goberdhan, A. Görgens, S. M. Gorski, D. W. Greening, J. C. Gross, A. Gualerzi, G. N. Gupta, D. Gustafson, A. Handberg, R. A. Haraszti, P. Harrison, H. Hegyesi, A. Hendrix, A. F. Hill, F. H. Hochberg, K. F. Hoffmann, B. Holder, H. Holthofer, B. Hosseinkhani, G. Hu, Y. Huang, V. Huber, S. Hunt, A. G.-E. Ibrahim, T. Ikezu, J. M. Inal, M. Isin, A. Ivanova, H. K. Jackson, S. Jacobsen, S. M. Jay, M. Jayachandran, G. Jenster, L. Jiang, S. M. Johnson, J. C. Jones, A. Jong, T. Jovanovic-Talisman, S. Jung, R. Kalluri, S.-i. Kano, S. Kaur, Y. Kawamura, E. T. Keller, D. Khamari, E. Khomyakova, A. Khvorova, P. Kierulf, K. P. Kim, T. Kislinger, M. Klingeborn, D. J. Klinke, M. Kornek, M. M. Kosanović, Á. F. Kovács, E.-M. Krämer-Albers, S. Krasemann, M. Krause, I. V. Kurochkin, G. D. Kusuma, S. Kuypers, S. Laitinen, S. M. Langevin, L. R. Languino, J. Lannigan, C. Lässer, L. C. Laurent, G. Lavieu, E. Lázaro-Ibáñez, S. Le Lay, M.-S. Lee, Y. X. F. Lee, D. S. Lemos, M. Lenassi, A. Leszczynska, I. T. S. Li, K. Liao, S. F. Libregts, E. Ligeti, R. Lim, S. K. Lim, A. Linē, A. Linnemannstöns, A. Llorente, C. A. Lombard, M. J. Lorenowicz, Á. M. Lörincz, J. Lötvall, J. Lovett, M. C. Lowry, X. Loyer, Q. Lu, B. Lukomska, T. R. Lunavat, S. L. N. Maas, H. Malhi, A. Marcilla, J. Mariani, J. Mariscal, E. S. Martens-Uzunova, L. Martin-Jaular, M. C. Martinez, V. R. Martins, M. Mathieu, S. Mathivanan, M. Maugeri, L. K. McGinnis, M. J. McVey, D. G. Meckes, K. L. Meehan, I. Mertens, V. R. Minciacchi, A. Möller, M. M. Jørgensen, A. Morales-Kastresana, J. Morhayim, F. Mullier, M. Muraca, L. Musante, V. Mussack, D. C. Muth, K. H. Myburgh, T. Najrana, M. Nawaz, I. Nazarenko, P. Nejsum, C. Neri, T. Neri, R. Nieuwland, L. Nimrichter, J. P. Nolan, E. N. M. N.-t. Hoen, N. N. Hooten, L. O'Driscoll, T. O'Grady, A. O'Loghlen, T. Ochiya, M. Olivier, A. Ortiz, L. A. Ortiz, X. Osteikoetxea, O. Østergaard, M. Ostrowski, J. Park, D. M. Pegtel, H. Peinado, F. Perut, M. W. Pfaffl, D. G. Phinney, B. C. H. Pieters, R. C. Pink, D. S. Pisetsky, E. P. von Strandmann, I. Polakovicova, I. K. H. Poon, B. H. Powell, I. Prada, L. Pulliam, P. Quesenberry, A. Radeghieri, R. L. Raffai, S. Raimondo, J. Rak, M. I. Ramirez, G. Raposo, M. S. Rayyan, N. Regev-Rudzki, F. L. Ricklefs, P. D. Robbins, D. D. Roberts, S. C. Rodrigues, E. Rohde, S. Rome, K. M. A. Rouschop, A. Rughetti, A. E. Russell, P. Saá, S. Sahoo, E. Salas-Huenuleo, C. Sánchez, J. A. Saugstad, M. J. Saul, R. M. Schiffelers, R. Schneider, T. H. Schøyen, A. Scott, E. Shahaj, S. Sharma, O. Shatnyeva, F. Shekari, G. V. Shelke, A. K. Shetty, K. Shiba, P. R. M. Siljander, A. M. Silva, A. Skowronek, O. L. Snyder, R. P. Soares, B. W. Sódar, C. Soekmadji, J. Sotillo, P. D. Stahl, W. Stoorvogel, S. L. Stott, E. F. Strasser, S. Swift, H. Tahara, M. Tewari, K. Timms, S. Tiwari, R. Tixeira, M. Tkach, W. S. Toh, R. Tomasini, A. C. Torrecilhas, J. P. Tosar, V. Toxavidis, L. Urbanelli, P. Vader, B. W. M. van Balkom, S. G. van der Grein, J. Van Deun, M. J. C. van Herwijnen, K. Van Keuren-Jensen, G. van Niel, M. E. van Royen, A. J. van Wijnen, M. H. Vasconcelos, I. J. Vechetti, T. D. Veit, L. J. Vella, É. Velot, F. J. Verweij, B. Vestad, J. L. Viñas, T. Visnovitz, K. V. Vukman, J. Wahlgren, D. C. Watson, M. H. M. Wauben, A. Weaver, J. P. Webber, V. Weber, A. M. Wehman, D. J. Weiss, J. A. Welsh, S. Wendt, A. M. Wheelock, Z. Wiener, L. Witte, J. Wolfram, A. Xagorari, P. Xander, J. Xu, X. Yan, M. Yáñez-Mó, H. Yin, Y. Yuana, V. Zappulli, J. Zarubova, V. Žékas, J.-y. Zhang, Z. Zhao, L. Zheng, A. R. Zheutlin, A. M. Zickler, P. Zimmermann, A. M. Zivkovic, D. Zocco, E. K. Zuba-Surma, Minimal Information for Studies of Extracellular Vesicles 2018 (MISEV2018): A Position statement of the International Society for Extracellular Vesicles and update of the MISEV2014 guidelines. *J. Extracell. Vesicles* **7**, 1535750 (2018).

2. C. Lasser, S. C. Jang, J. Lotvall, Subpopulations of extracellular vesicles and their therapeutic potential. *Mol. Aspects Med.* **60**, 1–14 (2018).

3. G. S. Hussey, C. Pineda Molina, M. C. Cramer, Y. Y. Tyurina, V. A. Tyurin, Y. C. Lee, S. O. El-Mossier, M. H. Murdock, P. S. Timashev, V. E. Kagan, S. F. Badylak, Lipidomics and RNA sequencing reveal a novel subpopulation of nanovesicle within extracellular matrix biomaterials. *Sci. Adv.* **6**, eaay4361 (2020).

4. D. Kim, H.-K. Woo, C. Lee, Y. Min, S. Kumar, V. Sunkara, H.-G. Jo, Y. J. Lee, J. Kim, H. K. Ha, Y.-K. Cho, EV-Ident: Identifying Tumor-Specific Extracellular Vesicles by Size Fractionation and Single-Vesicle Analysis. *Anal. Chem.* **92**, 6010–6018 (2020).

5. H. Zheng, S. Guan, X. Wang, J. Zhao, M. Gao, X. Zhang, Deconstruction of Heterogeneity of Size-Dependent Exosome Subpopulations from Human Urine by Profiling N-Glycoproteomics and Phosphoproteomics Simultaneously. *Anal. Chem.* **92**, 9239–9246 (2020).

6. M. C. Edman, S. R. Janga, S. S. Kakan, C. T. Okamoto, D. Freire, D. Feigenbaum, M. Lew, S. F. Hamm-Alvarez, Tears—More to them than meets the eye: Why tears are a good source of biomarkers in Parkinson's disease. *Biomark. Med.* **14**, 151–163 (2020).

7. E. Ponzini, C. Santambrogio, A. De Palma, P. Mauri, S. Tavazzi, R. Grandori, Mass spectrometry-based tear proteomics for noninvasive biomarker discovery. *Mass Spectrom. Rev.* **41**, 842–860 (2022).

8. A. Barmada, S. A. Shippy, Tear analysis as the next routine body fluid test. *Eye (Lond.)* **34**, 1731–1733 (2020).

9. T. Zhang, L. Hu, H. Ma, F. Ni, F. Liu, H. Chen, Detection of Tear Components Using Matrix-Assisted Laser Desorption Ionization/Time-of-Flight Mass Spectrometry for Rapid Dry Eye Diagnosis. *J. Proteome Res.* **19**, 3644–3651 (2020).

10. C. Rossi, I. Cicalini, M. C. Cufaro, L. Agnifili, L. Mastropasqua, P. Lanuti, M. Marchisio, V. De Laurenzi, P. Del Boccio, D. Pieragostino, Multi-Omics Approach for Studying Tears in Treatment-Naïve Glaucoma Patients. *Int. J. Mol. Sci.* **20**, 4029 (2019).

11. T. Takeuchi, K. Mori, H. Sunayama, E. Takano, Y. Kitayama, T. Shimizu, Y. Hirose, S. Inubushi, R. Sasaki, H. Tanino, Antibody-Conjugated Signaling Nanocavities Fabricated by Dynamic Molding for Detecting Cancers Using Small Extracellular Vesicle Markers from Tears. *J. Am. Chem. Soc.* **142**, 6617–6624 (2020).

12. K. Mori, M. Hirase, T. Morishige, E. Takano, H. Sunayama, Y. Kitayama, S. Inubushi, R. Sasaki, M. Yashiro, T. Takeuchi, A Pretreatment-Free, Polymer-Based Platform Prepared by Molecular Imprinting and Post-Imprinting Modifications for Sensing Intact Exosomes. *Angew. Chem. Int. Ed. Engl.* **58**, 1612–1615 (2019).

13. D. Pieragostino, P. Lanuti, I. Cicalini, M. C. Cufaro, F. Ciccocioppo, M. Ronci, P. Simeone, M. Onofrj, E. van der Pol, A. Fontana, M. Marchisio, P. Del Boccio, Proteomics Characterization of Extracellular Vesicles Sorted by Flow Cytometry Reveals a Disease-Specific Molecular Cross-Talk from Cerebrospinal Fluid and Tears in Multiple Sclerosis. *J. Proteomics* **204**, 103403 (2019).

14. L. Hu, T. Zhang, H. Ma, Y. Pan, S. Wang, X. Liu, X. Dai, Y. Zheng, L. P. Lee, F. Liu, Discovering the Secret of Diseases by Incorporated Tear Exosomes Analysis via Rapid-Isolation System: iTEARS. *ACS Nano* **16**, 11720–11732 (2022).

15. Y. Chen, Q. Zhu, L. Cheng, Y. Wang, M. Li, Q. Yang, L. Hu, D. Lou, J. Li, X. Dong, L. P. Lee, F. Liu, Exosome Detection via the Ultrafast-Isolation System: EXODUS. *Nat. Methods* **18**, 212–218 (2021).

16. C. Yeung Ching-Yan, F. Dondelinger, M. Schoof Erwin, B. Georg, Y. Lu, Z. Zheng, J. Zhang, J. Hannibal, J. Fahrenkrug, M. Kjaer, Circadian regulation of protein cargo in extracellular vesicles. *Sci. Adv.* **8**, eabc9061 (2022).

17. A. L. Wozniak, A. Adams, K. E. King, W. Dunn, L. K. Christenson, W.-T. Hung, S. A. Weinman, The RNA binding protein FMR1 controls selective exosomal miRNA cargo loading during inflammation. *J. Cell Biol.* **219**, e201912074 (2020).

18. G. van Niel, G. D'Angelo, G. Raposo, Shedding light on the cell biology of extracellular vesicles. *Nat. Rev. Mol. Cell Biol.* **19**, 213–228 (2018).

19. G. Li, S. He, L. Chang, H. Lu, H. Zhang, H. Zhang, J. Chiu, GADD45α and annexin A1 are involved in the apoptosis of HL-60 induced by resveratrol. *Phytomedicine* **18**, 704–709 (2011).

20. G. Koopman, C. P. Reutelingsperger, G. A. Kuijten, R. M. Keehnen, S. T. Pals, M. H. van Oers, Annexin V for flow cytometric detection of phosphatidylserine expression on B cells undergoing apoptosis. *Blood* **84**, 1415–1420 (1994).

21. P. Banerjee, V. Chander, A. Bandyopadhyay, Balancing functions of annexin A6 maintain equilibrium between hypertrophy and apoptosis in cardiomyocytes. *Cell Death Dis.* **6**, e1873 (2015).

22. S. Muraoka, M. Hirano, J. Isoyama, S. Nagayama, T. Tomonaga, J. Adachi, Comprehensive proteomic profiling of plasma and serum phosphatidylserine-positive extracellular vesicles reveals tissue-specific proteins. *iScience* **25**, 104012 (2022).

23. C. J. Jackson, K. G. Gundersen, L. Tong, T. P. Utheim, Dry eye disease and proteomics. *Ocul. Surf.* **24**, 119–128 (2022).

24. C. S. De Paiva, A. L. Villarreal, R. M. Corrales, H. T. Rahman, V. Y. Chang, W. J. Farley, M. E. Stern, J. Y. Niederkorn, D. Q. Li, S. C. Pflugfelder, Dry eye-induced conjunctival epithelial squamous metaplasia is modulated by interferon-gamma. *Invest. Ophth. Vis. Sci.* **48**, 2553–2560 (2007).

25. D. N. Stephens, N. A. McNamara, Altered Mucin and Glycoprotein Expression in Dry Eye Disease. *Optom. Vis. Sci.* **92**, 931–938 (2015).

26. R.-J. Ren, E. B. Dammer, G. Wang, N. T. Seyfried, A. I. Levey, Proteomics of protein post-translational modifications implicated in neurodegeneration. *Transl. Neurodegener.* **3**, 23 (2014).

27. R. J. Berckmans, A. Sturk, L. M. van Tienen, M. C. Schaap, R. Nieuwland, Cell-derived vesicles exposing coagulant tissue factor in saliva. *Blood* **117**, 3172–3180 (2011).

28. A. Comitato, P. Subramanian, G. Turchiano, M. Montanari, S. P. Becerra, V. Marigo, Pigment epithelium-derived factor hinders photoreceptor cell death by reducing intracellular calcium in the degenerating retina. *Cell Death Dis.* **9**, 560 (2018).

29. T. Vogl, M. Eisenblatter, T. Voller, S. Zenker, S. Hermann, P. van Lent, A. Faust, C. Geyer, B. Petersen, K. Roebrock, M. Schafers, C. Bremer, J. Roth, Alarmin S100A8/S100A9 as a biomarker for molecular imaging of local inflammatory activity. *Nat. Commun.* **5**, 4593 (2014).

30. M. Uhlen, L. Fagerberg, B. M. Hallstrom, C. Lindskog, P. Oksvold, A. Mardinoglu, A. Sivertsson, C. Kampf, E. Sjostedt, A. Asplund, I. Olsson, K. Edlund, E. Lundberg, S. Navani, C. A. Szigyarto, J. Odeberg, D. Djureinovic, J. O. Takanen, S. Hober, T. Alm, P.-H. Edqvist, H. Berling, H. Tegel, J. Mulder, J. Rockberg, P. Nilsson, J. M. Schwenk, M. Hamsten, K. von

Feilitzen, M. Forsberg, L. Persson, F. Johansson, M. Zwahlen, G. von Heijne, J. Nielsen, F. Ponten, Tissue-based map of the human proteome. *Science* **347**, 1260419 (2015).

31. M. Karlsson, C. Zhang, L. Mear, W. Zhong, A. Digre, B. Katona, E. Sjostedt, L. Butler, J. Odeberg, P. Dusart, F. Edfors, P. Oksvold, K. von Feilitzen, M. Zwahlen, M. Arif, O. Altay, X. Li, M. Ozcan, A. Mardinoglu, L. Fagerberg, J. Mulder, Y. Luo, F. Ponten, M. Uhlen, C. Lindskog, A single-cell type transcriptomics map of human tissues. *Sci. Adv.* **7**, eabh2169 (2021).

32. S. K. Vorperian, M. N. Moufarrej, C. Tabula Sapiens, S. R. Quake, Cell types of origin of the cell-free transcriptome. *Nat. Biotechnol.* **40**, 855–861 (2022).

33. B. Walcott, The Lacrimal Gland and Its Veil of Tears. *News Physiol. Sci.* **13**, 97–103 (1998).

34. C. Bissig, J. Gruenberg, ALIX and the multivesicular endosome: ALIX in Wonderland. *Trends Cell Biol.* **24**, 19–25 (2014).

35. H. Zhang, D. Freitas, H. S. Kim, K. Fabijanic, Z. Li, H. Chen, M. T. Mark, H. Molina, A. B. Martin, L. Bojmar, J. Fang, S. Rampersaud, A. Hoshino, I. Matei, C. M. Kenific, M. Nakajima, A. P. Mutvei, P. Sansone, W. Buehring, H. Wang, J. P. Jimenez, L. Cohen-Gould, N. Paknejad, M. Brendel, K. Manova-Todorova, A. Magalhaes, J. A. Ferreira, H. Osorio, A. M. Silva, A. Massey, J. R. Cubillos-Ruiz, G. Galletti, P. Giannakakou, A. M. Cuervo, J. Blenis, R. Schwartz, M. S. Brady, H. Peinado, J. Bromberg, H. Matsui, C. A. Reis, D. Lyden, Identification of distinct nanoparticles and subsets of extracellular vesicles by asymmetric flow field-flow fraction-ation. *Nat. Cell Biol.* **20**, 332–343 (2018).

36. H. Liu, W. Yuan, Q. Pang, C. Xue, X. Yan, Single-Particle Analysis of Tear Fluid Reveals Abundant Presence of Tissue Factor-Exposing Extracellular Vesicles with Strong Coagula-tion Activity. *Talanta* **239**, 123089 (2021).

37. S. Notomi, K. Ishihara, N. E. Efstathiou, J. J. Lee, T. Hisatomi, T. Tachibana, E. K. Konstantinou, T. Ueta, Y. Murakami, D. E. Maidana, Y. Ikeda, S. Kume, H. Terasaki, S. Sonoda, J. Blanz, L. Young, T. Sakamoto, K. H. Sonoda, P. Saftig, T. Ishibashi, J. W. Miller, G. Kroemer, D. G. Vavvas, Genetic LAMP2 deficiency accelerates the age-associated formation of basal laminar deposits in the retina. *Proc. Natl. Acad. Sci. U.S.A.* **116**, 23724–23734 (2019).

38. J. V. Ferreira, A. da Rosa Soares, J. Ramalho, C. Máximo Carvalho, M. H. Cardoso, P. Pintado, A. S. Carvalho, H. C. Beck, R. Matthiesen, M. Zuzarte, H. Girão, G. van Niel, P. Pereira, LAMP2A regulates the loading of proteins into exosomes. *Sci. Adv.* **8**, eabm1140 (2022).

39. Y. Zhu, H. Pick, N. Gasilova, X. Li, T.-E. Lin, H. P. Laeubli, A. Zippelius, P.-C. Ho, H. H. Girault, MALDI Detection of Exosomes: A potential tool for cancer studies. *Chem* **5**, 1318–1336 (2019).

40. G. Stubiger, M. D. Nairn, T. K. Abban, M. E. Openshaw, L. Mancera, B. Herzig, M. Wuczkowski, D. Senfter, R. M. Mader, MALDI-MS protein profiling of chemoresistance in extracellular vesicles of cancer cells. *Anal. Chem.* **90**, 13178–13182 (2018).

41. L. Kumar, M. E. Futschik, Mfuzz: A software package for soft clustering of microarray data. *Bioinformation* **2**, 5–7 (2007).

42. K. X. Wan, I. Vidavsky, M. L. Gross, Comparing similar spectra: From similarity index to spectral contrast angle. *J. Am. Soc. Mass Spectrom.* **13**, 85–88 (2002).

43. Y. Zhu, L. Qiao, M. Prudent, A. Bondarenko, N. Gasilova, S. B. Moller, N. Lion, H. Pick, T. Gong, Z. Chen, P. Yang, L. T. Lovey, H. H. Girault, Sensitive and fast identification of bacteria in blood samples by immunoaffinity mass spectrometry for quick BSI diagnosis. *Chem. Sci.* **7**, 2987–2995 (2016).